Significance of Rotating Ground Motions on Behavior of Symmetric- and Asymmetric-Plan Structures: Part I. Single-Story Structures

**Juan C. Reyes[a) and Erol Kalkan,[b) M.EERI

The California Building Code requires at least two ground motion components for the three-dimensional (3-D) response history analysis (RHA) of structures. For near-fault sites, these records should be rotated to fault-normal/fault-parallel (FN/FP) directions, and two RHA analyses should be performed separately. This approach is assumed to lead to two sets of responses that envelope the range of possible responses over all non-redundant rotation angles. This assumption is examined here using 3-D computer models of single-story structures having symmetric and asymmetric plans subjected to a suite of bi-directional earthquake ground motions. The influence that the rotation angle has on several engineering demand parameters is investigated in linear and non-linear domains to evaluate the use of the FN/FP directions, and the maximum direction (MD). The statistical evaluation suggests that RHAs should be conducted by rotating a set of records to the MD and FN/FP directions, and taking the maximum response values from these analyses as design values. [DOI: 10.1193/072012EQS241M]

INTRODUCTION

In the United States, both the International Building Code (ICBO 2015) and the California Building Code, CBC2013 (ICBO 2013), refer to ASCE/SEI 7-10 Chapter 16 (ASCE 2010) when response history analysis (RHA) is used for design validation of building structures. These guidelines require at least two horizontal ground motion components for three-dimensional (3-D) RHA. According to section 1615A.1.25 of the CBC2013, at sites within 5 km (3.1 miles) of the active fault that dominates the earthquake hazard, each pair of ground motion components shall be rotated to the fault-normal and fault-parallel (FN/FP) directions for 3-D RHAs. It is believed that the angle corresponding to the FN/FP directions will lead to the most critical structural response. This assumption is based on the fact that in the proximity of an active fault system, ground motions are significantly affected by the faulting mechanism, direction of rupture propagation relative to the site, and the possible static deformation of the ground surface associated with fling-step effects (Bray and Rodriguez-Marek 2004, Kalkan and Kunnath 2006), and these near-source effects cause most of the seismic energy from the rupture to arrive in a single coherent long-period

35 pulse of motion in the FN/FP directions (Mavroeidis and Papageorgiou 2003; Kalkan and
36 Kunnath 2007, 2008). Thus, rotating ground motion pairs to FN/FP directions is assumed to
37 be a conservative approach, appropriate for design verification of new building structures.

38   The provision for rotating ground motion records to FN/FP directions has been intro-
39 duced in the most recent ASCE/SEI 7-10 (ASCE 2010) standards, which have additional
40 changes incorporated in the new generation of the building codes. One of the changes is
41 the use of maximum-direction (MD) ground motion, a revised definition of horizontal ground
42 motions used for site-specific ground motion procedures for seismic design (Chapter 21 of
43 ASCE/SEI 7-10). The MD, the direction of the rotated ground motion pair, leads to peak
44 linear response quantity of a single lumped mass oscillator free to vibrate in both horizontal
45 directions. The assumptions behind the MD ground motions are that the structural properties
46 including stiffness and strength are identical in all directions, and the azimuth of the MD
47 ground motion coincides with the structure's principal axes (Singh et al. 2011). While
48 the first assumption may be true for purely symmetric-plan structures (such as oil tanks,
49 communication poles, elevated water tanks, guyed towers etc.), it may not be valid for
50 other systems in which response is dominated by modes of vibration along specific axes.
51 The second assumption, on the other hand, refers to ground motions with a lower probability
52 of occurrence—it is very unlikely that ground motion incidence angle (angle of attack) with
53 respect to the building's transverse direction is same as the MD.

54   For linear single-degree-of-freedom (SDOF) systems, MD retains the characteristics
55 of pulse-like motions and provides an upper bound (in the maximum direction) and a
56 lower bound (in the minimum direction) spectral response (Zamora and Riddell 2011).
57 In Chapter 21 of the ASCE/SEI 7-10, the concept of MD is used to develop a MD response
58 spectrum to be used for seismic design. In the MD response spectrum, spectral ordinates at
59 each period can be in a different orientation because the maximum motion varies with the
60 period of the oscillator. Because of these issues, use of MD ground motions for seismic
61 design is found to be controversial, and it is argued that it would result in 10% to 30% over-
62 estimation of design ground motion level (Stewart et al. 2011).

63   The idea of rotating ground motion pairs to certain axes, critical for response, is not new; it
64 has been studied previously in various contexts. Penzien and Watabe (1974) defined the prin-
65 cipal axis of a pair of ground motions as the angle or axis at which the two horizontal com-
66 ponents are uncorrelated, and as being independent of the vibration period. It is also shown
67 that the principal axis is not associated with the MD (Hong and Goda 2010). Using this idea of
68 principal axes, the effects of seismic rotation angle—defined as the angle between the prin-
69 cipal axes of the ground motion pair and the structural axes—have been comprehensively
70 investigated (e.g., Fernandez-Davila et al. 2000; MacRae and Matteis 2000; Tezcan and
71 Alhan 2001; Khoshnoudian and Poursha 2004; Rigato and Medina 2007; Lagaros 2010;
72 Zamora and Riddell 2011; Kalkan and Kwong 2012, 2014; Goda 2012). The previous studies
73 demonstrate that the rotation angle of ground motions influences the structural response sig-
74 nificantly and that the angle that yields the peak response over all possible non-redundant
75 angles, called $\theta_{critical}$ (or θ_{cr}), depends on the seismic excitation level and character of shaking.

76   A formula for deriving θ_{cr} was proposed by Wilson (1995). Other researchers
77 have improved on the closed-form solution of Wilson (1995) by accounting for the
78 statistical correlation of horizontal components of ground motion in an explicit way

(Lopez and Torres 1997, Lopez et al. 2000). However, Wilson's formula is based on concepts from response spectrum analysis—an approximate procedure used to estimate structural response in the linear domain. Focusing on linear multi-degree-of-freedom (MDOF) sym- metric- and asymmetric-plan structures, Athanatopoulou (2005) investigated the effect of the rotation angle on structural response using RHAs, and provided formulas for determining the maximum response over all rotation angles given the linear response histories for two orthogonal orientations. The analysis results have shown that, for the records used, the critical value of an engineering-demand parameter (EDP) can be up to 80% larger than the usual response produced when the as-recorded ground motion components are applied along the structural axes. Athanatopoulou (2005) also concluded that the critical angle corresponding to peak response over all angles varies not only with the ground motion pair under considera- tion, but also with the response quantity of interest. These findings are confirmed in Kalkan and Kwong (2012, 2014) where the impacts of ground motion rotation angle including those corresponding to the FN/FP directions on several different EDPs are shown based on a linear 3-D computer model of a six-story instrumented building.

The previous studies investigated response behavior of either linear MDOF buildings or nonlinear response of single-degree-of-freedom (SDOF) systems subjected to two compo- nents of ground motion. Because there is still a lack of research addressing bi-directional nonlinear response of realistic MDOF systems considering ground motion directionality effects, this study systematically evaluates whether ground motions rotated to MD or FN/FP directions lead to conservative[*] estimates of EDPs from RHAs. For this purpose, 3-D computer models of single-story structures having symmetric (torsionally stiff) and asymmetric (torsionally flexible) layouts are subjected to an ensemble of bi-directional near-fault ground motions with and without apparent velocity pulses. Also investigated are the rotation angle of an apparent velocity pulse, and its correlation with the MD and FN/FP directions. At the end, this study provides practical recommendations towards the use of MD and FN/FP directions to rotate ground motion records for RHA of building struc- tures. The companion paper (Kalkan and Reyes 2015) presents further validations using 3-D computer models of nine-story structures having symmetric and asymmetric layouts sub- jected to the same ground motion set.

GROUND MOTIONS SELECTED

Thirty near-fault ground motion records selected for this investigation (listed in Table 1) were recorded from nine shallow crustal earthquakes compatible with the following hazard conditions:

- Moment magnitude: $M_w = 6.7 \pm 0.2$
- Closest fault distance from a site to co-seismic rupture plane: 0.1 km to 15 km
- National Earthquake Hazards Reduction Program (NEHRP) site class: C or D
- Highest usable period[†] $\geq 6\,\text{s}$

---

[*]The term, conservative, is used here either peak or close to peak EDP values.
[†]Low-cut corner frequency of the Butterworth filter applied; because the highest usable period is greater than 6 sec, records in Table 1 have enough long period content to compute their spectra reliably up to 6 sec.

Table 1. Selected near-fault ground motion records

Record sequence number	Earthquake name	Year	Station name	Earthquake magnitude (M_w)	Style of Faulting	Closest fault distance (km)
1	Gazli, USSR	1976	Karakyr	6.8	Thrust	5.5
2	Imperial Valley-06	1979	Aeropuerto Mexicali	6.5	Strike-slip	0.3
3	Imperial Valley-06	1979	Agrarias	6.5	Strike-slip	0.7
4	Imperial Valley-06	1979	Bonds Corner	6.5	Strike-slip	2.7
5	Imperial Valley-06	1979	EC Meloland Overpass FF	6.5	Strike-slip	0.1
6	Imperial Valley-06	1979	El Centro Array #6	6.5	Strike-slip	1.4
7	Imperial Valley-06	1979	El Centro Array #7	6.5	Strike-slip	0.6
8	Irpinia, Italy-01	1980	Auletta	6.9	Normal	9.6
9	Irpinia, Italy-01	1980	Bagnoli Irpinio	6.9	Normal	8.2
10	Irpinia, Italy-01	1980	Sturno	6.9	Normal	10.8
11	Nahanni, Canada	1985	Site 1	6.8	Thrust	9.6
12	Nahanni, Canada	1985	Site 2	6.8	Thrust	4.9
13	Nahanni, Canada	1985	Site 3	6.8	Thrust	5.3
14	Superstition Hills-02	1987	Parachute Test Site	6.5	Strike-slip	1.0
15	Superstition Hills-02	1987	Westmorland Fire Sta	6.5	Strike-slip	13.0
16	Loma Prieta	1989	BRAN	6.9	Reverse	10.7
17	Loma Prieta	1989	Gilroy Array #3	6.9	Reverse	12.8
18	Loma Prieta	1989	LGPC	6.9	Reverse	3.9
19	Loma Prieta	1989	San Jose – St. Teresa Hills	6.9	Reverse	14.7
20	Loma Prieta	1989	Saratoga – Aloha Ave	6.9	Reverse	8.5
21	Loma Prieta	1989	Saratoga – W Valley Coll.	6.9	Reverse	9.3
22	Erzincan, Turkey	1992	Erzincan	6.7	Strike-slip	4.4
23	Northridge-01	1994	Jensen Filter Plant Gen.	6.7	Reverse	5.4
24	Northridge-01	1994	Newhall – Fire Sta	6.7	Reverse	5.9
25	Northridge-01	1994	Newhall – W Pico Can. Rd.	6.7	Reverse	5.5
26	Northridge-01	1994	Pacoima Dam (downstr)	6.7	Reverse	7.0
27	Northridge-01	1994	Rinaldi Receiving Sta	6.7	Reverse	6.5
28	Northridge-01	1994	Sylmar – Olive V. Med FF	6.7	Reverse	5.3
29	Kobe, Japan	1995	KJMA	6.9	Reverse	1.0
30	Kobe, Japan	1995	Nishi-Akashi	6.9	Reverse	7.1

Because the number of ground motions recorded within 5 km of causative faults is limited in ground motion databases, the distance limit is extended up to 15 km with the premise that ground motions do not attenuate significantly within 15 km of rupture plane for the earthquake magnitude range considered (e.g., Campbell and Bozorgnia 2007, Segou and Kalkan 2011, Graizer and Kalkan 2015). These ground motions were rotated to fault-normal (FN) and fault-parallel (FP) orientations using the following transformation equations:

$$\ddot{u}_{FP} = \ddot{u}_1 \cos(\beta_1) + \ddot{u}_2 \cos(\beta_2) \tag{1}$$

$$\ddot{u}_{FN} = \ddot{u}_1 \sin(\beta_1) + \ddot{u}_2 \sin(\beta_2) \tag{2}$$
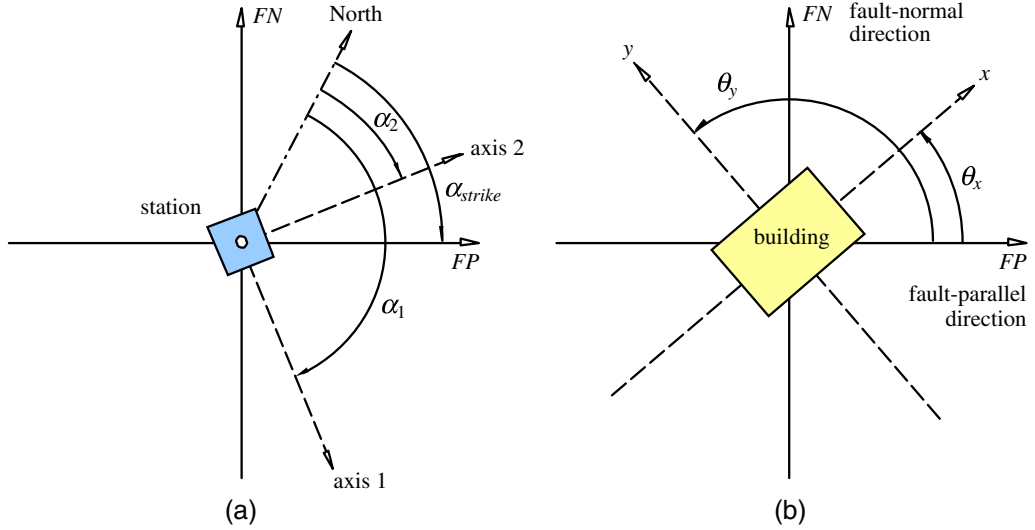
Figure 1. (a) Reference axes for the fault and the instrument, with relevant angles noted. (b) Reference axis for the building.

where $\beta_1 = \alpha_{strike} - \alpha_1$, $\beta_2 = \alpha_{strike} - \alpha_2$, α_{strike} is the strike of the fault, and α_1 and α_2 are the azimuths of the instrument axes, as shown in Figure 1a. The geometric mean or median spectrum[‡] of 30 FN records is taken as the target spectrum for the design of single-story symmetric and asymmetric structures to be used in a parametric study. The ground motions (acceleration time series) were additionally rotated θ_x away from the FP axis, as shown in Figure 1b. The angle θ_x varies from 5° to 360° at every 5° in the counterclockwise direction. These rotations were conducted using Equations 1 and 2, with β_1 and β_2 redefined as $\beta_1 = \alpha_{strike} - \alpha_1 - \theta_x$ and $\beta_2 = \alpha_{strike} - \alpha_2 - \theta_y$. The x- and y-axes, as well as the angles θ_x and θ_y, are shown in Figure 1b.

Figure 2 shows the response of a two-degrees-of-freedom system with equal stiffness and damping ratio in the x- and y-axes subjected to the FN/FP components of a ground motion ($\theta_x = 0$). The maximum deformation of this system occurs at an angle θ_m rotated counterclockwise from the FP axis. As mentioned above, this orientation is called maximum-direction. The maximum radial deformation in Figure 2 could also be obtained by analyzing a SDOF system subjected to only the MD rotated ground motion.

For 30 near-fault ground motion pairs, Figure 3 shows the polar plots of spectral acceleration values as a function of the rotation angle θ_x for elastic SDOF systems with vibration period (T_n) equal to 0.2 s, 1 s, 2 s, 3 s, and 5 s. Each dot (color coded according to distance from fault rupture) indicates θ_m of the MD ground motion pair and corresponding linear response of the SDOF system (A_m). In each polar plot, there are 30 dots (purple, black, and green). We took the median of the response values from 30 MD ground motion

---

[‡]Because we assume that the data is log-normally distributed, the geometric mean and the median are the same.
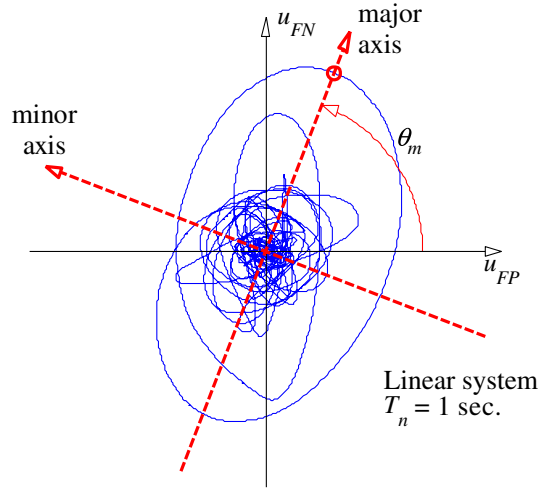
Figure 2. Trace of deformation orbit of a two-degrees-of-freedom system with direction-independent stiffness and damping subjected to the FN/FP components of a ground motion.

pairs; this median value is the radius of the blue circle and blue dashed circles representing the 16th and 84th percentile. Similarly, the red curves represent the median spectral acceleration value $\pm$ one standard deviation (σ_n). Spectral accelerations are scaled to the number labeled on the upper-right corner of each plot; this number is the radius of the largest circle. Except for short period system ($T_n = 0.2$ s), median spectral acceleration values A_n (red curves) tend to be polarized with the fault-normal ($\theta_x = 90°$) direction.

Studies of ground motion directionality have shown that the azimuth of the MD ground motion is arbitrary for fault distances larger than approximately 3–5 km (Campbell and Bozorgnia 2007, Watson-Lamprey and Boore 2007). At closer fault distances (closer than 3–5 km), however, the azimuth of the maximum-direction motion tends to align with the strike-normal direction (Watson-Lamprey and Boore 2007, Huang et al. 2008). In contrast, θ_m (purple dots corresponding to those MD records within 5 km of fault rupture) in Figure 3 clearly shows large scattering with no visible correlation with the FN direction.

It should be also noted that spectral acceleration values, A_m, corresponding to the maximum-direction angle, θ_m, are generally higher than the median spectral acceleration value A_n.

POLARIZATON OF VELOCITY PULSES WITH FAULT-NORMAL/ FAULT-PARALLEL AND MAXIMUM DIRECTIONS

Baker (2007) developed a numerical procedure to identify and characterize velocity pulses for ground motion records. This procedure was used here to identify velocity pulses in rotated motions at each rotation angle θ_x. Figure 4 shows polar plots of identified velocity-pulse periods and spectral accelerations as a function of θ_x for the records that contain velocity pulses. In these plots, the red dots indicate pulse periods scaled in polar coordinates and
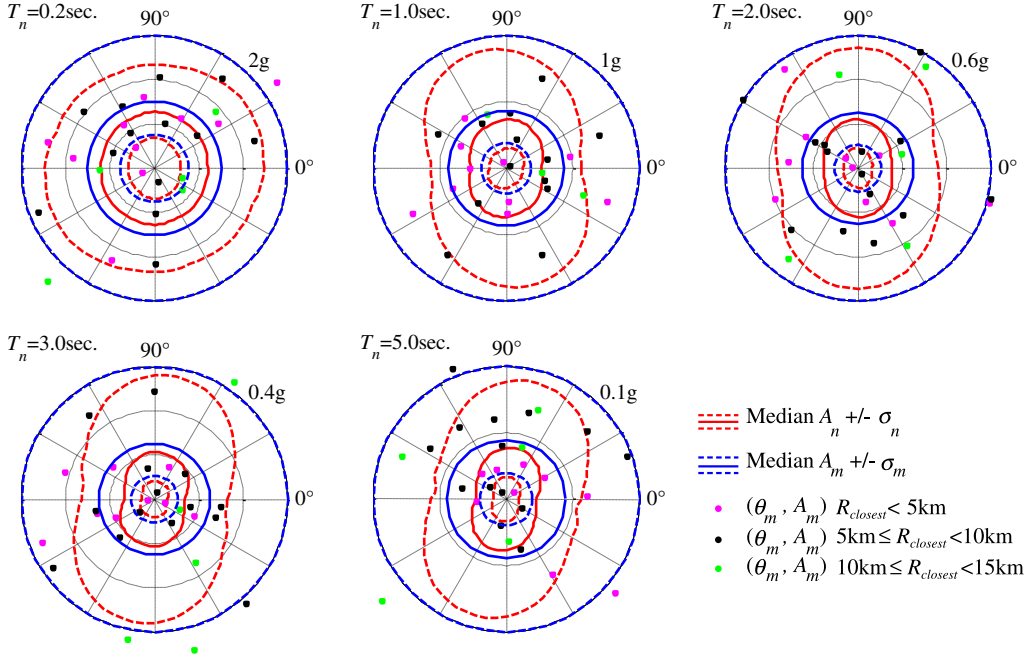
Figure 3. For 30 near-fault ground motion pairs, polar plots of spectral accelerations as a function of the rotation angle θ_x are shown for linear SDOF systems with vibration period (T_n) equal to 0.2 s, 1 s, 2 s, 3 s, and 5 s (damping ratio 5%). The red curves represent the median spectral acceleration value $(A_n) \pm \sigma_n$ (solid line is for median, and dash lines are for 16th and 84th percentile; log-normal distribution is used). The purple, black and green points (color distinguished based on closest fault distance) correspond to pairs of maximum-direction angle θ_m and spectral acceleration values A_m. The blue circles represent the median spectral acceleration value $\pm\sigma_m$ in the maximum direction. Note that except for short period SDOF system ($T_n = 0.2$ s), A_n values are generally polarized with fault-normal (90°) direction; on the contrary, θ_m shows large scattering with no correlation with fault-normal (90°) direction.

167 the directions in which the velocity pulses are identified. The filled gray area shows ranges of
168 θ_x with velocity pulses. The dashed blue curves show spectral accelerations computed for a
169 SDOF system with T_n equal to the maximum pulse period of the ground motion (GM) at a
170 5% damping ratio (e.g., dashed blue curves for GM1 correspond to spectral accelerations
171 computed for a SDOF system with $T_n = 4.9$ s). The blue line identifies the maximum-
172 direction angle θ_m. The numerical values for maximum pulse periods and maximum spectral
173 accelerations are presented in the upper right corner of each sub-plot. This figure presents
174 important findings. For example, polar plot for the GM1 (left upper corner in Figure 4)
175 indicates that the apparent velocity pulses are identified for θ_x in between 40°–80° and
176 130°–170°, and the pulse disappears at other angles including 90° (fault-normal direction).
177 For this record, the maximum-direction angle, θ_m, is computed at 45° and 135° in which the
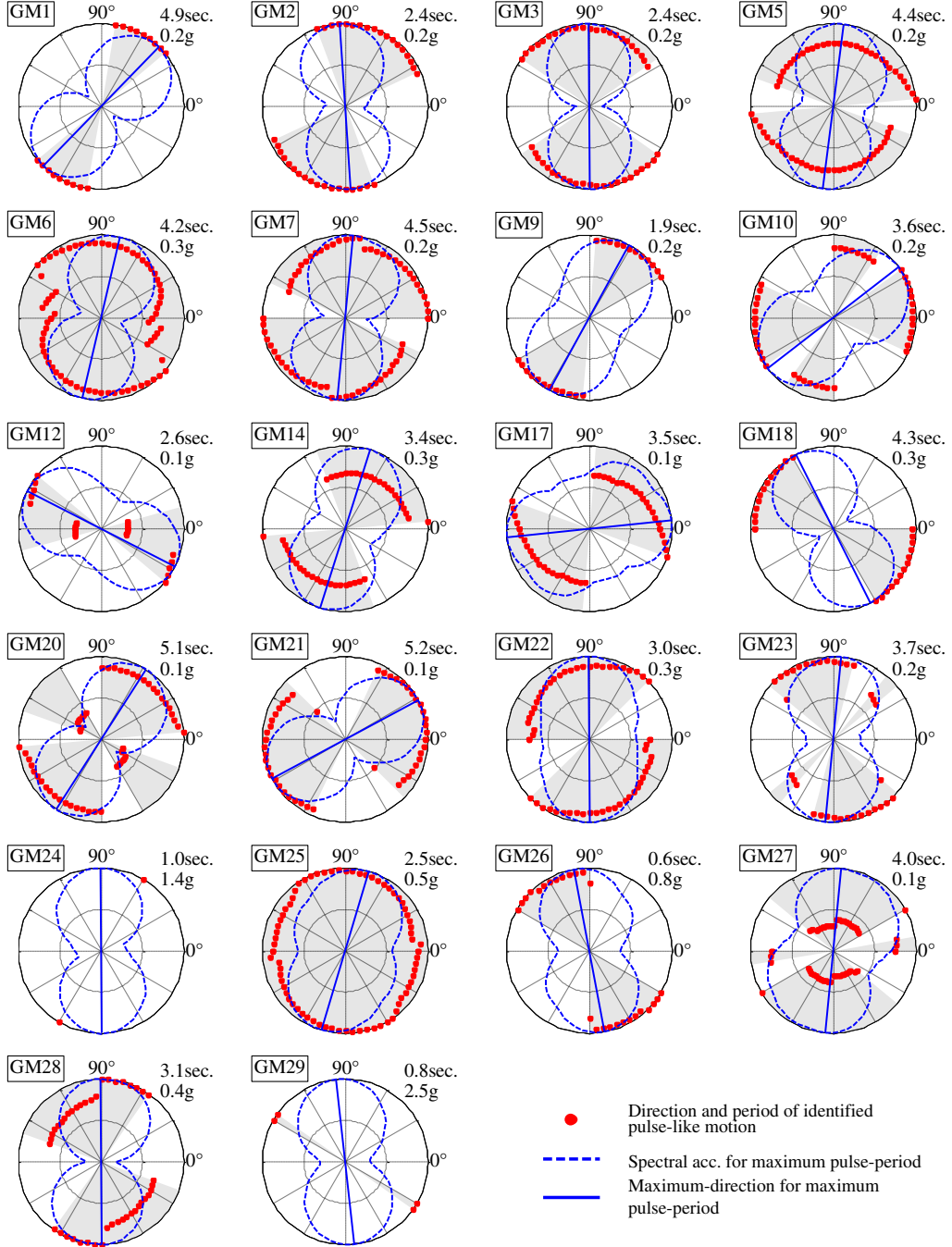178 velocity pulse is also identified. Lastly, a maximum spectral acceleration of 0.2 g is observed

Figure 4. Polar plots of identified velocity-pulse periods and spectral accelerations (damping ratio 5%) as a function of the rotation angle θ_x for 22 ground motion (GM) pairs. The red dots show the directions in which velocity pulses are identified with their corresponding pulse periods. The filled gray area shows range of θ_x with velocity pulses. The dashed blue curves show spectral acceleration values for the maximum identified pulse period. The blue solid line identifies the maximum direction. Numerical values for maximum pulse periods and maximum spectral accelerations are presented in the upper right corner of each sub-plot.

179 at θ_m. In the FN direction, the maximum spectral acceleration is decreased by 30% and equals
180 0.14 g. Examinations of polar plots of all records permit the following observations:

1. The velocity pulses are identified for 22 out of 30 records (approximately 75% of the complete set of records). Seven records with velocity pulses identified at some rotation angles have no pulses in the FN direction (within $\pm 2.5°$ of 90°), indicating that the FN direction does not always have an apparent velocity pulse, as also demonstrated by Zamora and Riddell (2011).

2. For almost all ground motion pairs, the maximum-direction angle, θ_m, is in the range of directions that the velocity pulses are identified. This strong correlation shows that the maximum spectral acceleration almost always occurs in the direction at which the velocity pulse is observed.

3. FN direction and MD angle θ_m coincide (within $\pm 5°$) for 9 records out of 22 records having velocity pulses (approximately 40% of records with velocity pulses), indicating that approximately 60% of the time, maximum spectral acceleration takes place in directions other than the FN direction for those records with apparent velocity pulses.

4. For a given ground motion pair, the rotation angle θ_x may alter the maximum pulse period significantly (for example GM6), showing that the pulse period of rotated components varies with θ_x.

DESCRIPTION OF STRUCTURAL SYSTEMS AND COMPUTER MODELS

199 The structural systems selected for this investigation are 30 single-story buildings with
200 three-degrees-of-freedom. Their vibration periods T_n are equal to 0.2 s, 1 s, 2 s, 3 s, and 5 s.
201 The yield strength reduction factors R are equal to 3, 5, and a value that leads to linear design
202 (i.e., $R = 1.0$ for the strongest ground motion in the dataset; $R < 1.0$ for rest of the records).
203 The lateral load–resisting system of the buildings consists of buckling-restrained braces
204 (BRBs) with non-moment-resisting beam-column connections. The plan shapes and bracing
205 layouts are shown in Figure 5. The buildings are identified by the letters A and B depending
206 on the plan shape; plan A is rectangular with two axes of symmetry (torsionally stiff), while
207 plan B is asymmetric (torsionally flexible) about both x- and y-axes. The design spectrum was
208 taken as the geometric mean (median) of the 5% damped spectral acceleration response spec-
209 tra of the FN components of the 30 records. The earthquake design forces were determined by
210 bi-directional linear response spectrum analysis of the building, with the design spectrum
211 reduced by a response modification factor R. The constitutive model used for the BRBs
212 is the simplified trilinear model shown in Figure 6. This model was obtained based on experi-
213 mental results (Merritt et al. 2003). The parameters, k and q_y, are the same for all BRBs of
214 a building. Plots of mode shapes and effective modal masses presented in Reyes and Kalkan
215 (2012) permit the following observations: (1) Lateral displacements dominate motion of the
216 A-plan (symmetric-plan) buildings in modes 1 and 2, whereas torsion dominates motion in
217 the third mode. This indicates weak coupling between lateral and torsional components of
218 motion. Additionally, the period of the dominantly torsional mode is much shorter than the
219 period of the dominantly lateral modes, a property representative of buildings with lateral
220 load–resisting systems located along the perimeter of the plan. (2) Coupled lateral-torsional
221 motions occur in the first and third modes of the plan B (asymmetric-plan) buildings, whereas
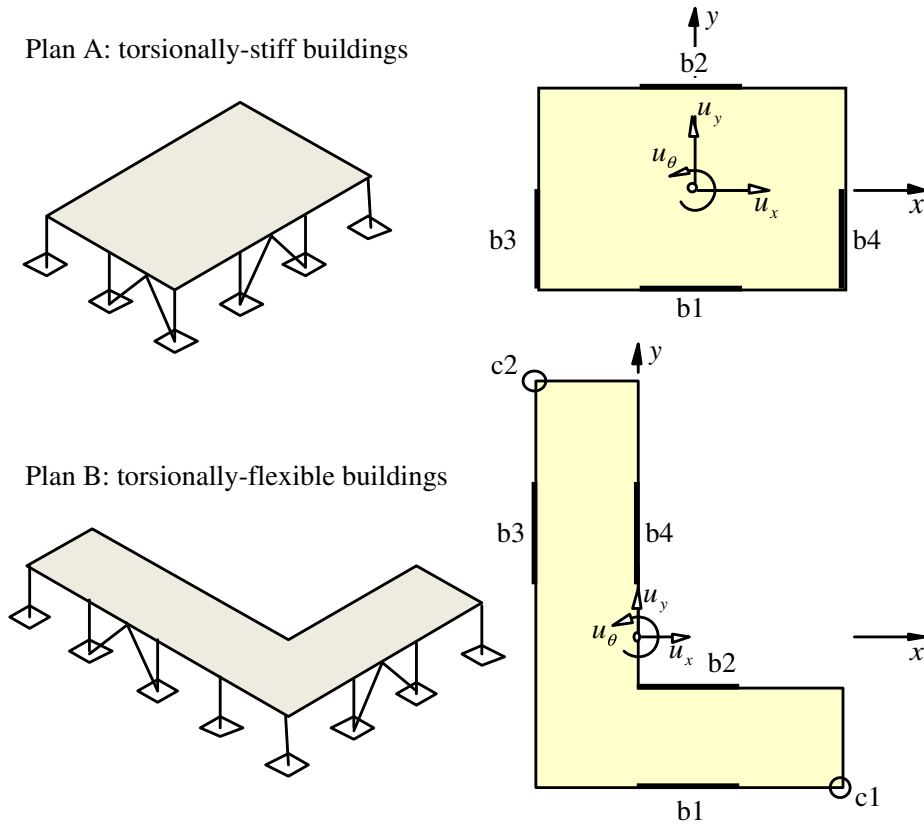
Plan A: torsionally-stiff buildings

Plan B: torsionally-flexible buildings

Figure 5. Schematic isometric and plan views of the selected single-story structural systems with three-degrees-of-freedom noted; BRBs are highlighted as b1…4.
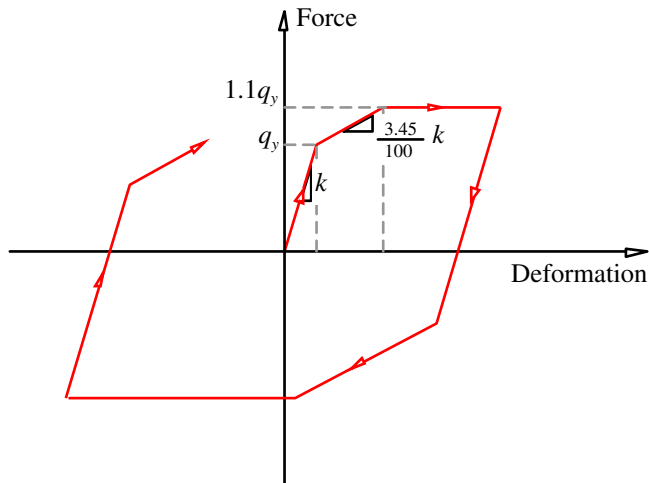

Figure 6. Constitutive model used for BRBs.

222 lateral displacements dominate motion in the second mode; according to the ASCE/SEI 7-10
223 (ASCE 2010), plan B presents an extreme torsional irregularity. (3) The higher-mode con-
224 tributions to response are expected to be significant for the plan B buildings because the
225 effective mass of the first lateral modes is less than 40% of the total mass.

226   **EVALUATION METHODOLOGY**

227   The following steps were implemented for evaluating the significance of the ground
228 motion rotation angle on linear and nonlinear response behavior of single-story buildings
229 with symmetric and asymmetric plans located in near-fault sites:

230   1. For each of the 30 ground motion records selected, calculate rotated ground motion
231   components by varying θ_x from 0° to 360° at every 5° in the clockwise direction
232   (Figure 1b). In addition, calculate rotated ground motion components for $\theta_x = \theta_m$
233   and $\theta_x = \theta_m + 90°$ as explained earlier.
234   2. Calculate the 5% damped response spectrum $A(T)$ for the FN component of the 30
235   records at 300 logarithmically spaced periods T over the period range from 0.001 s
236   to 6 s.
237   3. Implement an iterative procedure for designing the 30 single-story systems
238   described previously using the median spectrum of 30 FN components of Step 2,
239   as the design spectrum. At the end of this step, values for parameters k and q_y are
240   obtained for each BRB. Recall that the single-story systems have vibration periods
241   T_n equal to 0.2 s, 1 s, 2 s, 3 s, and 5 s, and yield strength reduction factors R equal to
242   3, 5, and a value that leads to linear design.
243   4. Conduct linear and nonlinear RHAs of the 30 single-story symmetric- and
244   asymmetric-plan systems subjected to bi-directional rotated components of ground
245   motions obtained in step 1. For each RHA, obtain floor displacements, floor total
246   accelerations, BRB plastic deformations, and BRB forces. This step involves more
247   than 34,000 RHAs.

248   **RESULTS**

249   Selected EDPs for single-story systems are displacement, u_x and u_y; floor total accelera-
250 tion, $\ddot{u}_x^t$ and $\ddot{u}_y^t$, at the center of mass; member forces; and plastic deformation of selected
251 BRBs. Figure 7 shows floor total accelerations, $\ddot{u}_x^t$, at the center of mass (red curve) as a
252 function of the rotation angle, θ_x, for symmetric-plan buildings with $T_n = 2$ s, 3 s, and
253 5 s subjected to ground motions with velocity-pulse period close to T_n. The filled gray
254 area shows values of θ_x in which the velocity pulses are identified for each record. Note
255 that angles $\theta_x = 0°$ and 90° correspond to the FP and FN axes, respectively. For asym-
256 metric-plan systems, roof displacements u_x at the center of mass and member forces at bra-
257 cing b3 (Figure 5) as a function of the rotation angle θ_x are shown in Figure 8 and Figure 9,
258 respectively. Similar figures for other EDPs along the x- and y-axes are shown in Reyes and
259 Kalkan (2012). In these figures, the EDPs are normalized by their peak values in each polar
260 plot. These figures permit the following observations: (1) For symmetric-plan systems, the
261 maximum floor total acceleration, $\ddot{u}_x^t$, over all non-redundant orientations are generally polar-
262 ized in the direction in which apparent velocity pulse with period close to T_n is observed;
263 while this polarization is almost perfect for linear systems, it vanishes for nonlinear systems,
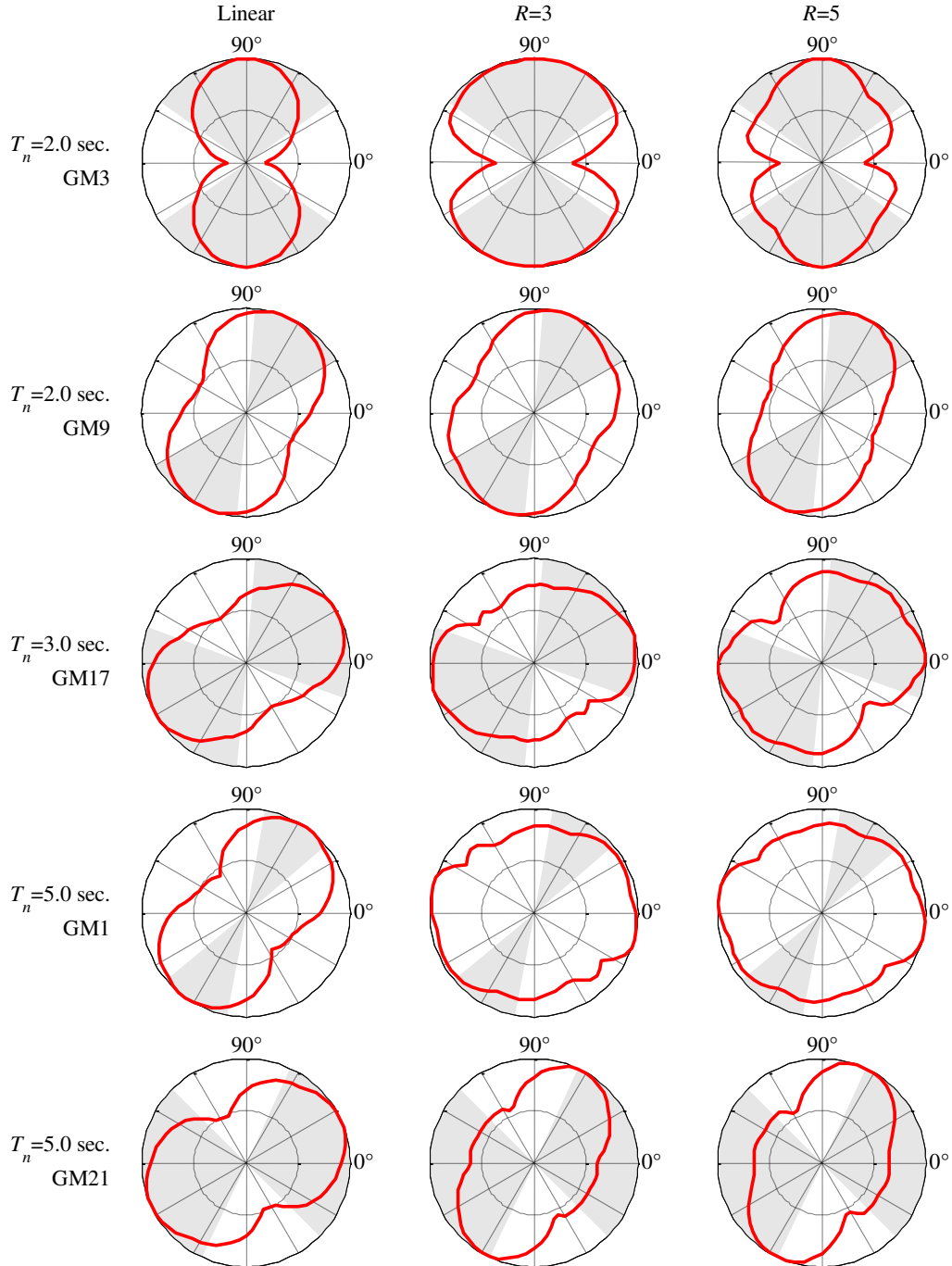
Figure 7. Floor total accelerations, $\ddot{u}^t{}_x$, at the center of mass (red curve) as a function of rotation angle θ_x for single-story symmetric-plan systems with $T_n = 2$ s, 3 s, and 5 s subjected to ground motions with velocity-pulse-period close to T_n. The filled gray area shows values of θ_x in which velocity pulses are identified. Angles $\theta_x = 0°$ and $90°$ correspond to the fault-parallel and fault-normal directions, respectively. Floor total accelerations are normalized by peak values in each polar plot.
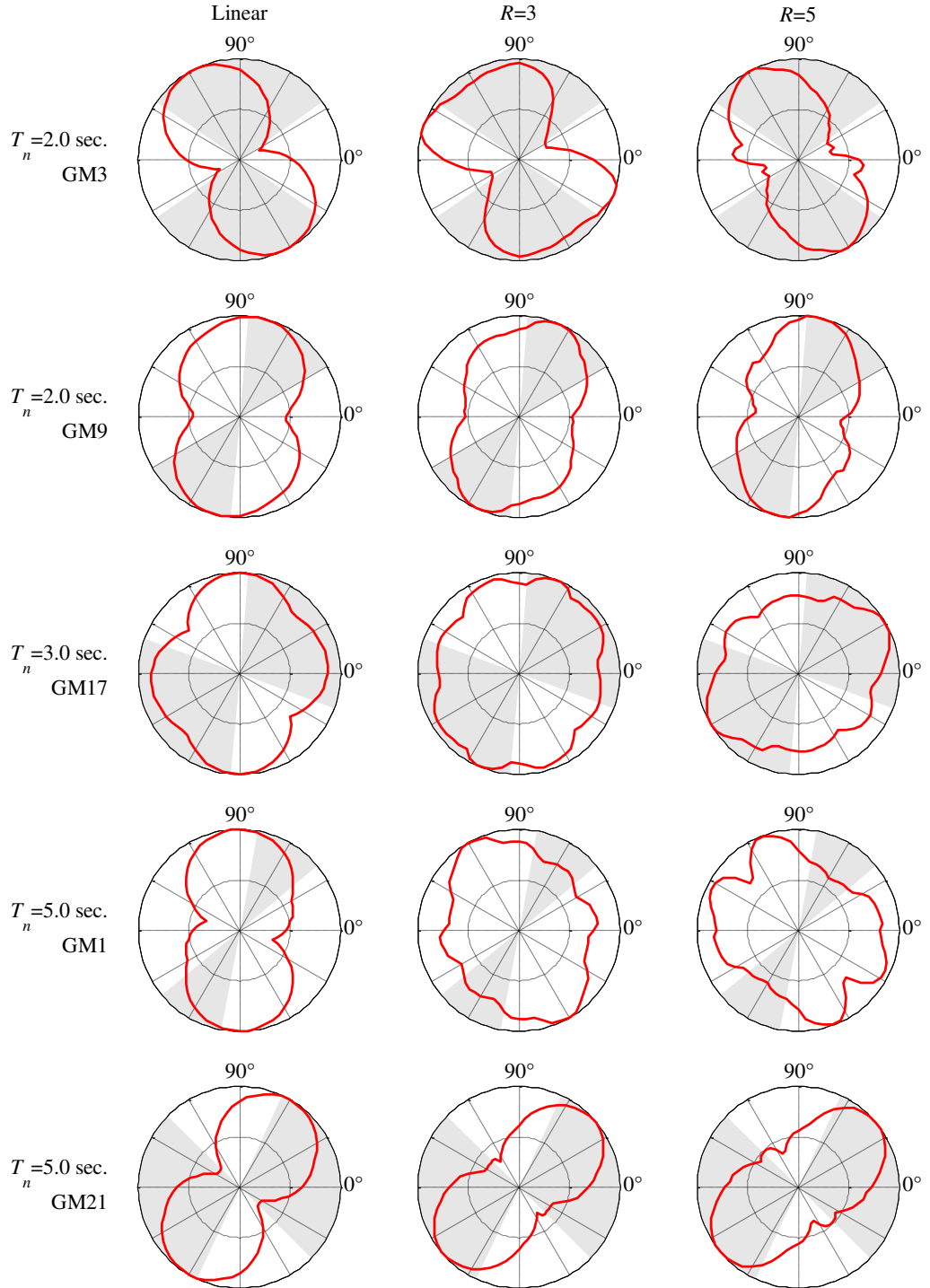
Figure 8. Displacement u_x at center of mass (red curve) as a function of rotation angle θ_x for single-story asymmetric-plan systems with $T_n = 2$ s, 3 s, and 5 s subjected to ground motions with velocity-pulse period close to T_n. The filled gray area shows values of θ_x in which velocity pulses are identified for each record. Angles $\theta_x = 0°$ and $90°$ correspond to the fault-parallel and fault-normal directions, respectively. Displacements are normalized by peak values in each polar plot.
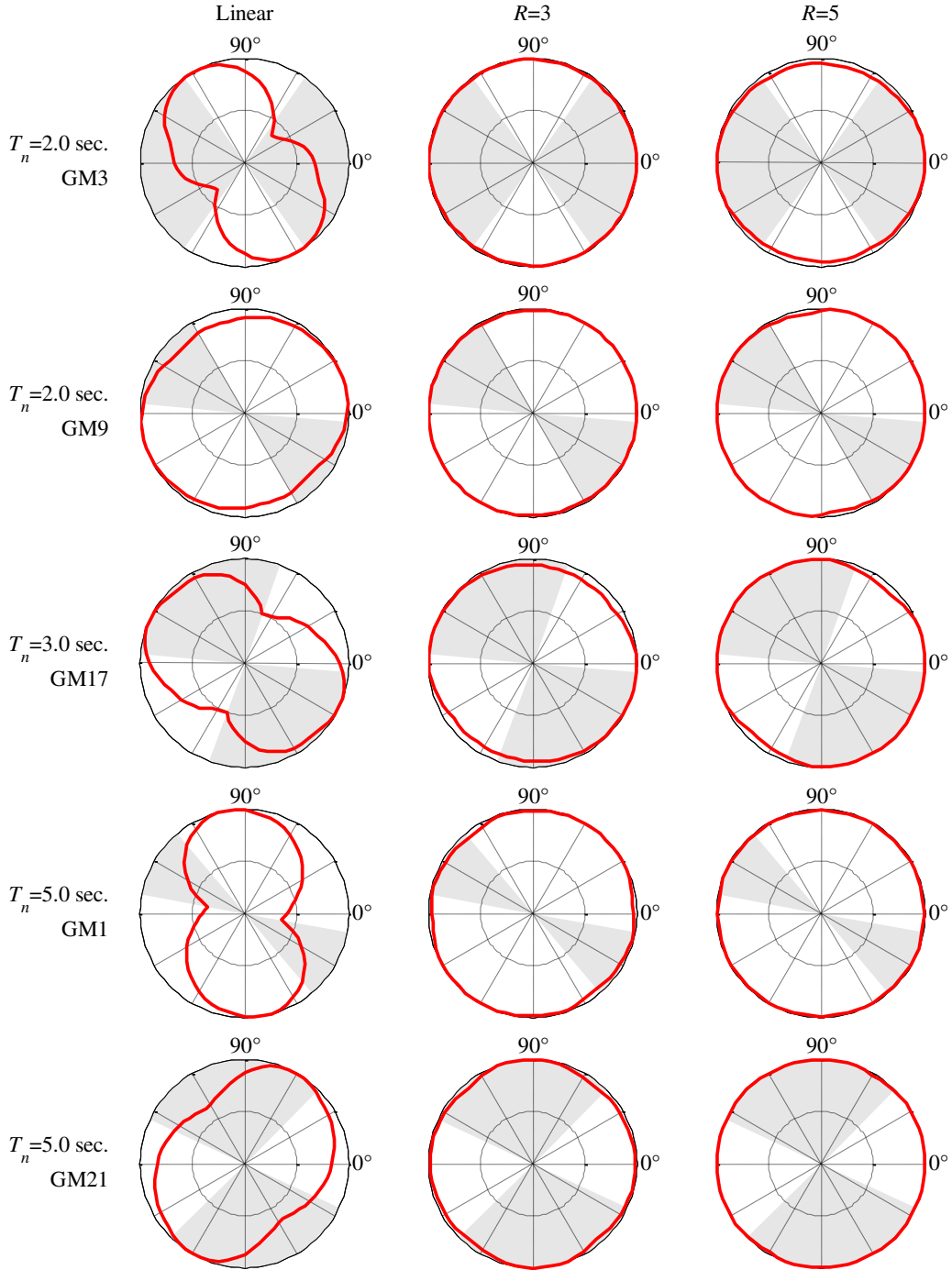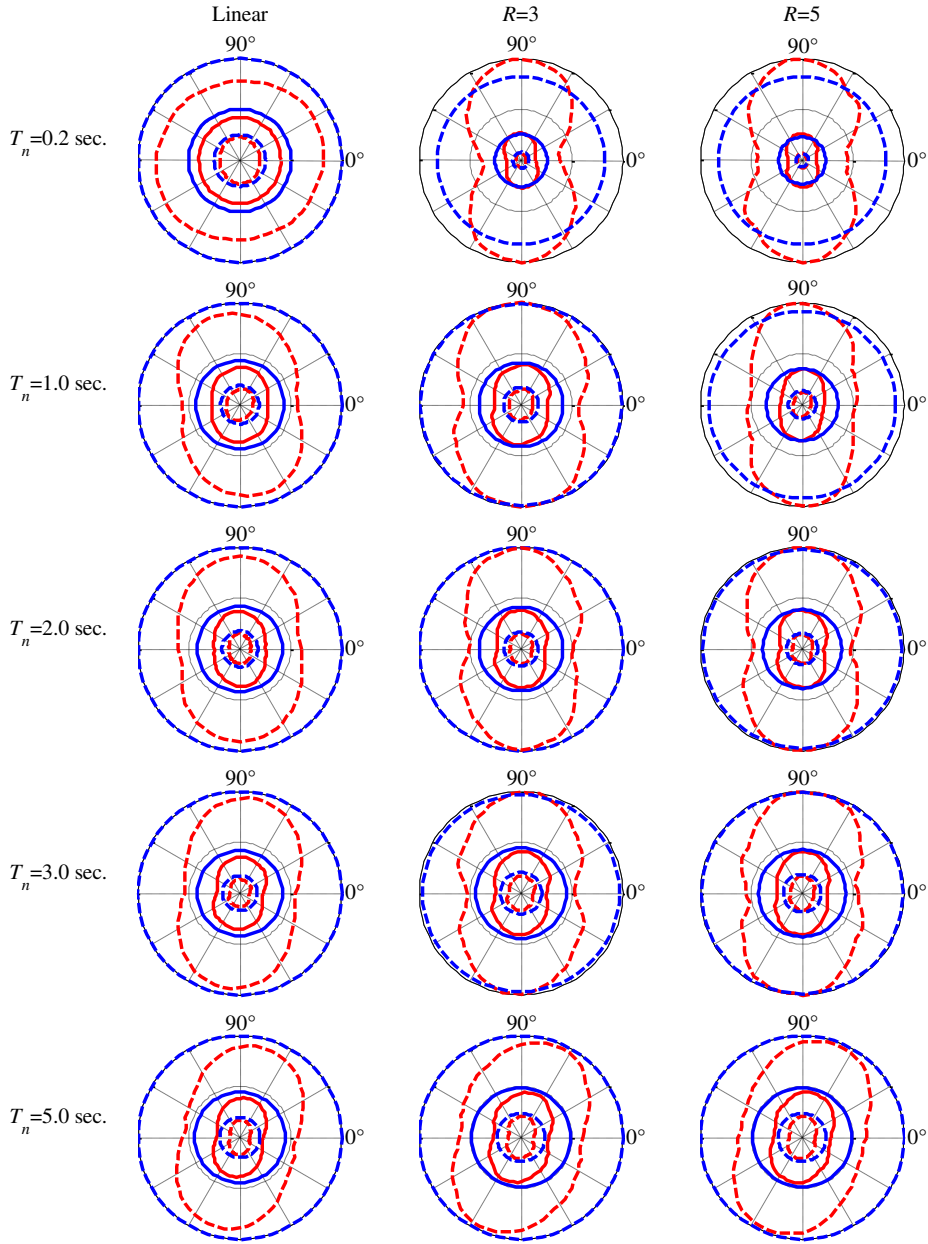
Figure 9. Force in bracing b3 (red curve) as a function of rotation angle, θ_x, for single-story asymmetric-plan systems with elastic first-mode vibration period $T_n = 2$ s, 3 s, and 5 s subjected to ground motions (GM) with velocity-pulse period close to T_n. The filled gray area shows values of θ_x in which velocity pulses are identified for each record. Angles $\theta_x = 0°$ and 90° correspond to the fault-parallel and fault-normal directions, respectively. Forces are normalized by peak values in each polar plot.

264 leading the maximum floor total acceleration $\ddot{u}_x^t$ to also occur in the direction different from
265 that of the velocity pulse (white areas in Figure 7); this is attributed to period elongation due
266 to inelastic action. For asymmetric-plan systems, however, no strong correlation is observed
267 between the orientation leading to maximum displacement u_x and the velocity-pulse direction
268 even for linear case. (2) Only for linear systems, the maximum force in selected BRBs is
269 polarized in the direction in which the pulse is identified (Figure 9), whereas for all nonlinear
270 systems, BRB reaches its ultimate capacity quickly without being influenced by the rotation
271 angle. (3) EDPs may be underestimated by more than 50% if a building is subjected to only
272 FN/FP components of a pulse-like ground motion; this observation is valid for both
273 symmetric- and asymmetric-plan systems (for example, last row in Figure 7 and Figure 8).
274 (4) There is no optimum orientation for a given structure; the rotation angle that leads to
275 maximum EDPs varies not only with the ground motion pair selected, but also with the period
276 and R value used in the design process of the building.

277   For a selected earthquake scenario, it is commonly assumed that EDPs are log-normally
278 distributed (Cornell et al. 2002). For this reason, it is more appropriate to represent the
279 "mean" structural response by the median; a conclusion that is widely accepted. Because
280 the geometric mean and median of a random variable having a log-normal distribution
281 are the same, we decided to employ the term "median" instead of geometric mean, as is
282 commonly done. Figure 10 shows the median displacements, u_x (normalized by their
283 peak values), at the center of mass as a function of the rotation angle, θ_x, for symmetric-
284 plan buildings with $T_n = 0.2$ s, 1 s, 2 s, 3 s, and 5 s, and with $R = 3$, 5 and a value that
285 leads to linear design subjected to 30 bi-directional ground motions. The red curves represent
286 the median displacement $u_x \pm$ one standard deviation (σ) computed based on peak response
287 values due to each ground motion pair at each non-redundant rotation angle. In these figures,
288 the blue circles represent the median MD displacement $(u_{mx} \pm \sigma)^§$ for the systems subjected
289 to ground motions only in the MD. Recall that MD stands for maximum direction. Note that
290 for a given ground motion pair, MD changes with period. In Figure 10, although the MD
291 displacement $u_{mx} \pm \sigma$ values correspond to a single value for each system, it is visualized as a
292 full circle to facilitate direct comparisons with median displacements $u_x \pm \sigma$, which is a func-
293 tion of the rotation angle θ_x. For the asymmetric-plan systems, plots for displacements at
294 corner c2 (Figure 5) are depicted in Figure 11. Median values of other EDPs are shown
295 in Reyes and Kalkan (2012). These figures provide an overall statistical examination to gen-
296 eralize the observations previously made based on individual records in Figures 7 thru 9.
297 These general observations are: (1) For short period ($T_n = 0.2$ s) linear symmetric- and asym-
298 metric-plan systems, maximum median-displacement values (red curves) are independent of
299 the ground motion rotation angle θ_x. At longer periods, however, maximum median displa-
300 cements are influenced by the rotation angle, and they are generally polarized with the FN
301 direction; this is more pronounced for symmetric-plan systems. For R values of 3 and 5, the
302 effect of the rotation angle on displacement is significant for all systems. (2) Median values of
303 floor total accelerations and member forces are generally not influenced by the ground
304 motion rotation angle in both linear and nonlinear range for both symmetric- and asymmetric-
305 plan buildings. (3) For all systems, it is clear that the R value used in the design process
306 affects the difference between the median MD displacement and the maximum median

---

§16th and 84th percentile values of u_{mx} are computed as $u_{mx}\, e^{\pm\sigma}$

Figure 10. Median displacements u_x at the center of mass as a function of rotation angle θ_x for single-story symmetric-plan systems with $T_n = 0.2$ s, 1 s, 2 s, 3 s, and 5 s subjected to bi-directional loading. The red curves represent the median displacement $u_x \pm \sigma$. The blue circles represent the median displacement $u_{xm} \pm \sigma$ for the systems subjected to bi-directional ground motions in the maximum direction. Displacements are normalized by peak values in each polar plot.
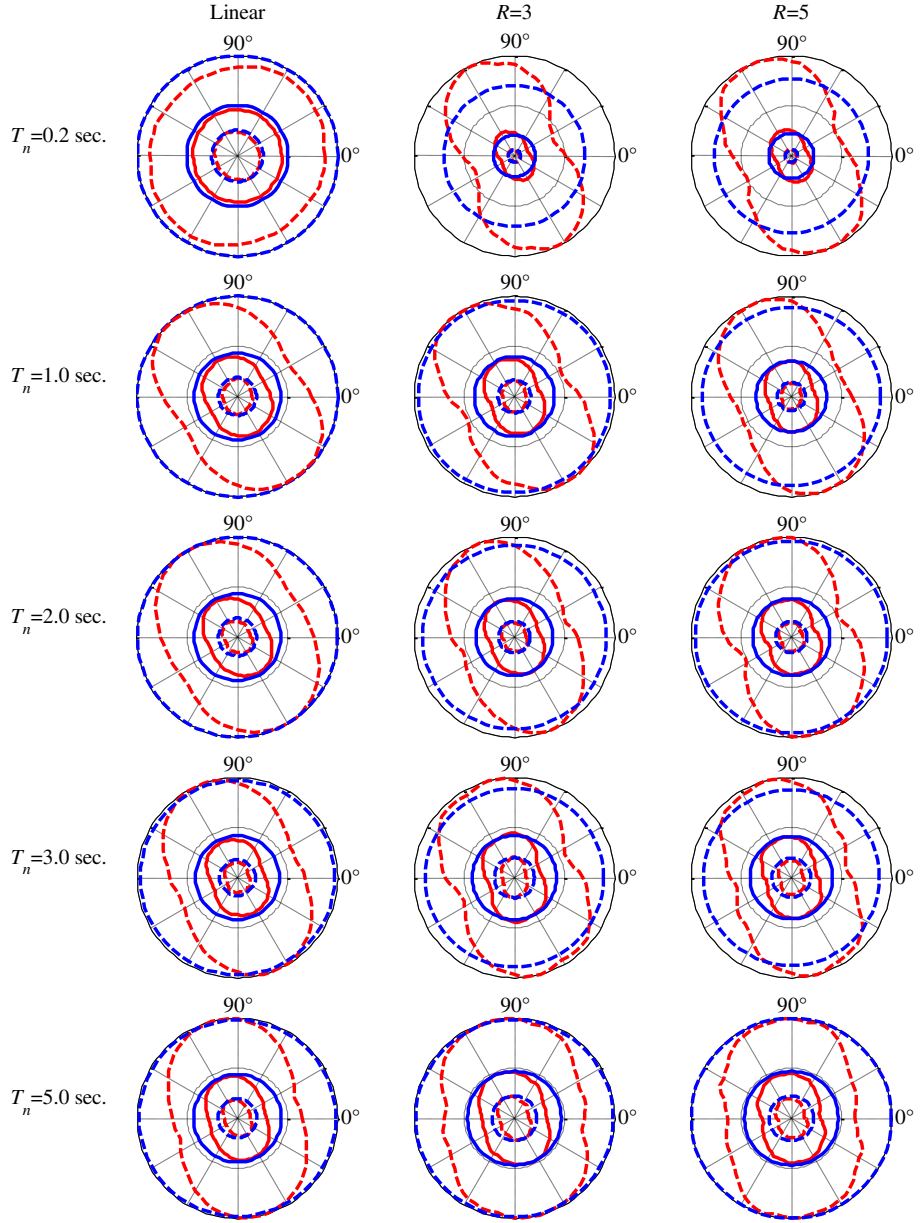
Median displacement +/- one standard deviation due to components rotated θ_x degrees
Median displacement +/- one standard deviation due to MD components

Figure 11. Median displacements u_x at corner c2 as a function of rotation angle θ_x for single-story asymmetric-plan systems with $T_n = 0.2$ s, 1 s, 2 s, 3 s, and 5 s subjected to bi-directional loading. The red curves represent the median displacement $u_x \pm \sigma$. The blue circles represent the median displacement $u_{xm} \pm \sigma$ for the systems subjected to bi-directional ground motions in the maximum direction. Displacements are normalized by peak values in each polar plot.

307 displacement over all non-redundant orientations. Maximum values of EDPs for linear sys-
308 tems are usually smaller than median MD EDPs—a conclusion also drawn by Huang et al.
309 (2008). However, for nonlinear systems, maximum median EDPs may be equal or larger than
310 MD EDPs. This is an important finding since it demonstrates that use of MD ground motions
311 does not necessarily provide over-conservative (or unrealistic) EDPs for systems responding
312 in nonlinear range in particular for asymmetric-plan structures.

313   Next, median percent error in estimation of peak median response over all rotation angles
314 due to MD or FN/FP directions rotated ground motions are computed as:

$$Error(\%) = \frac{\max(\hat{x}_{FN/FP}, \hat{x}_{MD}) - \hat{x}_{\max}}{\hat{x}_{\max}} \times 100 \tag{3}$$

315 where $\hat{x}_{\max}$ is the peak median EDP over all rotation angles. $\hat{x}_{MD}$ and $\hat{x}_{FN/FP}$ are the peak
316 median EDP due to MD or FN/FP directions rotated ground motions, respectively. The posi-
317 tive error means overestimation, and negative is the underestimation of peak median EDPs
318 from 30 ground motion pairs. Using Equation 3, the error values are computed for nonlinear
319 symmetric- and asymmetric-plan buildings and for EDPs shown in Figure 10 and Figure 11
320 along x- and y-axes; these results are tabulated in Table 2. The maximum value of under-
321 estimation and overestimation of peak median response when either MD or FN/FP directions
322 rotated ground motions are used are 9% and 8%, respectively. It is evident that conducting
323 nonlinear RHA for ground motions oriented in the FN/FP and MD directions does not always
324 lead to the peak value of median displacement over all non-redundant rotation angles. How-
325 ever, displacements are not underestimated or overestimated substantially (less than 10%) if
326 the system is subjected to MD and FN/FP directions of a large set of ground motions, and the
327 maximum response values from these analyses are taken as design values. The underestima-
328 tion could be as much as 50% if a single record is used.

Table 2. Percent error in estimation of peak median displacements over all rotation angles
using equation (3); positive error means overestimation, and negative underestimation (shown
with bold numbers).

Structure	Structural period (s)	x-direction			y-direction		
		Linear	$R = 3$	$R = 5$	Linear	$R = 3$	$R = 5$
Symmetric-plan	0.2	19%	−1%	**0%**	0%	−1%	**0%**
	1.0	17%	4%	0%	**0%**	−1%	−1%
	2.0	14%	7%	2%	−1%	0%	−1%
	3.0	17%	8%	5%	0%	**0%**	0%
	5.0	14%	8%	7%	−1%	−2%	−2%
Asymmetric-plan	9.0	**−14%**	**−9%**	1%	1%	**−8%**	−4%
	6.6	2%	0%	2%	0%	**−6%**	−4%
	3.7	**−2%**	2%	2%	−1%	0%	**−5%**
	7.8	**−1%**	−1%	5%	0%	−1%	**−6%**
	2.4	**−1%**	5%	1%	−2%	−1%	**0%**

329   **CONCLUSIONS**

330   In this study, the influence that the rotation angle of the ground motion has on several
331 engineering demand parameters has been examined systematically in linear and nonlinear
332 domains using a suite of 3-D computer models of symmetric- and asymmetric-plan
333 single-story buildings subjected to 30 bi-directional near-fault ground motion records.
334 The results presented herein suggest that:

335   • Velocity pulses in near-fault records may appear in directions different from the
336   maximum-direction (MD) or fault-normal and fault-parallel (FN/FP) directions.
337   For the near-fault records examined, MD shows large scattering with no visible
338   correlation with the FN/FP directions. This observation is valid even for motions
339   recorded within 5 km of the fault.
340   • For linear systems, the maximum displacement occurs in the direction in which
341   apparent velocity pulse with a period close to the fundamental period of the structure
342   is observed. This strong polarization vanishes for nonlinear systems due to period
343   elongation. These observations are valid for both symmetric- and asymmetric-plan
344   single-story buildings investigated.
345   • For a given ground motion pair, rotation angle leading to maximum elastic response
346   is different than that for maximum inelastic response; thus, any conclusions drawn
347   based on linear systems will not be applicable for nonlinear systems.
348   • For a given ground motion pair, there is no optimum orientation maximizing all
349   EDPs simultaneously; maximum EDP can happen in any direction different
350   from the direction of the velocity pulse. The critical angle, θ_{cr}, corresponding to
351   the largest response over all possible rotation angles, varies with the ground motion
352   pair selected, R value used in the design process, and the response quantity (EDP) of
353   interest. Therefore, it is difficult to determine an "optimal" building orientation that
354   maximizes demands for all EDPs before conducting RHAs.
355   • For a given ground motion pair, the use of FN/FP directions applied along the prin-
356   cipal directions of the building not always guarantees that the maximum response
357   over all possible angles will be obtained. Even though this approach may lead to a
358   maximum for one EDP, it may be non-conservative for other EDPs.
359   • Treating the as-recorded direction as a randomly chosen direction, it is observed that
360   there is more than a 50% chance for the larger response among the FN and FP values
361   to exceed the response corresponding to an arbitrary orientation. The latter observa-
362   tion is valid for most, but not for all, of the record pairs and response quantities
363   considered.
364   • For a given ground motion pair, MD is not unique; it changes with period and R
365   value of the system, as a result, the MD response spectrum becomes an envelope of
366   the maximum response spectral accelerations of the ground motion pair at all pos-
367   sible rotation angles and periods. It is therefore argued that the use of MD ground
368   motion for design is an overly conservative approach. While it can be true for linear
369   systems, conducting nonlinear RHA for ground motions oriented in the MD does
370   not always lead to maximum EDPs over all orientations in particular for
371   asymmetric-plan buildings.
372   • The conclusions drawn above are for a given ground motion pair. The statistical
373   evaluation based on the large set of ground motion pairs suggest that, for

374   practical applications in near-fault sites, RHAs should be conducted by rotating a
375   set of records to the MD (computed at building's first-mode period) and FN/FP
376   directions, and taking the maximum response values from these analyses as
377   design values. The results presented in our companion paper also support this
378   recommendation.
379 • We also recommend rotating ground motions to MD and FN/FP direction for sites
380   within 15 km of the fault instead of 5 km; the rational for this recommendation is
381   that propagating waves do not show notable attenuation within 15 km of the cau-
382   sative fault; thus their intensity and frequency content do not alter for events with
383   high seismic energy (moment magnitude > 7.0).

384   **ACKNOWLEDGMENTS**

389   **REFERENCES**

390   American Society of Civil Engineers (ASCE), 2010. *Minimum Design Loads for Buildings and*
391   *Other Structures, ASCE/SEI 7-10*, Reston, VA.
392   Athanatopoulou, A. M., 2005. Critical orientation of three correlated seismic components, *Engi-*
393   *neering Structures* **27**, 301–312.
394   Baker, J. W., 2007. Quantitative classification of near-fault ground motions using wavelet ana-
395   lysis, *Bulletin of the Seismological Society of America* **97**, 1486–1501.
396   Bray, J. D., and Rodriguez-Marek, A., 2004. Characterization of forward-directivity ground
397   motions in the near-fault region, *Soil Dynamics and Earthquake Engineering* **24**, 815–828.
398   Campbell, K. W., and Bozorgnia, Y., 2007. *Campbell-Bozorgnia NGA Ground Motion Relations*
399   *for the Geometric Mean Horizontal Component of Peak and Spectral Ground motion Para-*
400   *meters, PEER Report No. 2007-02*, University of California, Berkeley.
401   Cornell, C. A., Jalayer, F., Hamburger, R. O., and Foutch, D. A., 2002. Probabilistic basis for
402   2000 SAC federal emergency management agency steel moment frame guidelines, *Journal of*
403   *Structural Engineering*, ASCE, **128**, 526–533.
404   Fernandez-Davila, I., Comeinetti, S., and Cruz, E. F., 2000. Considering the bi-directional effects
405   and the seismic angle variations in building design, in *Proceedings of the 12th World Con-*
406   *ference on Earthquake Engineering*, Auckland, New Zealand.
407   Goda, K., 2012. Comparison of peak ductility demand of inelastic sdof systems in maximum
408   elastic response and major principal directions, *Earthquake Spectra* **28**, 385–399.
409   Graizer, V., and Kalkan, E., 2015. *Update of the Graizer-Kalkan Ground-Motion Prediction*
410   *Equations for Shallow Crustal Continental Earthquakes*, U.S. Geological Survey Open-
411   File Report 2015-1009, 79 pp., available at http://pubs.usgs.gov/of/2015/1009/.
412   Hong, H. P., and Goda, K., 2010. Characteristics of horizontal ground motion measures along
413   principal directions, *Earthquake Engineering and Engineering Vibration* **9**, 9–22.
414   Huang, Y., Whittaker, A. S., and Luco, N., 2008. Maximum spectral demands in the near-fault
415   region, *Earthquake Spectra* **24**, 319–34.

International Conference of Building Officials (ICBO), 2015. *California Building Code*, Whittier, CA.

Kalkan, E., and Kunnath, S.K., 2006. Effects of fling-step and forward directivity on the seismic response of buildings, *Earthquake Spectra* **22**, 367–390.

Kalkan, E., and Kunnath, S. K., 2007. Effective cyclic energy as a measure of seismic demand, *Journal of Earthquake Engineering* **11**, 725–751.

Kalkan, E., and Kunnath, S. K., 2008. Relevance of absolute and relative energy content in seismic evaluation of structures, *Advances in Structural Engineering* **11**, 17–34.

Kalkan, E., and Kwong, N. S., 2012. *Evaluation of Fault-normal/Fault-parallel Directions Rotated Ground motions for Response History Analysis of An Instrumented Six-story Building*, U.S. Geological Survey Open-File Report 2012–1058, 30 pp., available at http://pubs.usgs .gov/of/2012/1058/.

Kalkan, E., and Kwong, N. S., 2014. Pros and cons of rotating ground motion records to fault-normal/parallel directions for response history analysis of buildings, *Journal of Structural Engineering*, ASCE, **140**, 04013062.

Kalkan, E., and Reyes, J. C., 2015. Significance of rotating ground motions on behavior of symmetric- and asymmetric-plan structures: Part 2. multi-story structures, *Earthquake Spectra* **31**, XXX–XXX.

Khoshnoudian, F., and Poursha, M., 2004. Responses of three-dimensional buildings under bi-directional and unidirectional seismic excitations, in *Proceedings of the 13th World Conference on Earthquake Engineering*, Vancouver, Canada.

Lagaros, N. D., 2010. Multicomponent incremental dynamic analysis considering variable incident angle, *Structure and Infrastructure Engineering* **6**, 77–94.

Lopez, O. A., and Torres, R., 1997. The critical angle of seismic rotation and structural response, *Earthquake Engineering and Structural Dynamics* **26**, 881–894.

Lopez, O. A., Chopra, A. K., and Hernandez, J. J., 2000. Critical response of structures to multi-component earthquake excitation, *Earthquake Engineering and Structural Dynamics* **29**, 1759–1778.

MacRae, G. A., and Mattheis, J., 2000. Three-dimensional steel building response to near-fault motions, *Journal of Structural Engineering*, ASCE, **126**, 117–126.

Mavroeidis, G. P., and Papageorgiou, A. S., 2003. A mathematical representation of near-fault ground motions, *Bulletin of the Seismological Society of America* **93**(3), 1099–1131.

Merritt, S., Uang, C. M., and Benzoni, G., 2003. *Subassemblage Testing of Star Seismic Buckling Restrained Braces: Report No. TR-2003/04, Final Report to Star Seismic, LLC*, University of California, San Diego, CA.

Penzien, J., and Watabe, M., 1974. Characteristics of 3-dimensional earthquake ground motions, *Earthquake Engineering and Structural Dynamics* **3**, 365–373.

Reyes, J. C., and Kalkan, E., 2012. *Should Ground-Motion Records Be Rotated to Fault-Normal/Parallel or Maximum Direction for Response History Analysis of Buildings?* U.S. Geological Survey Open-File Report 2012–1261, 81 pp., available at http://pubs.usgs.gov/of/2012/1261/.

Rigato, A., and Medina, R. A., 2007. Influence of angle of rotation on the seismic demands for inelastic single-storey structures subjected to bi-directional ground motions, *Engineering Structures* **29**, 2593–2601.

Segou, M., and Kalkan, E., 2011. Ground Motion Attenuation during M7.1 Darfield and M6.3 Christchurch (New Zealand) Earthquakes and Performance of Global Predictive Models, *Seismological Research Letters* **82**, 866–874.

462 Singh, J. P., Porter, L. D., and Zafir, Z., 2011. A practitioner's perspective of ASCE/SEI 7-10
463   maximum-direction ground motions, in *Proceedings of the Annual Convention of Structural*
464   *Engineers Association of California*.
465 Stewart, J. P., Abrahamson, N. A., Atkinson, G. M., Baker, J., Boore, D. M., Bozorgnia, Y.,
466   Campbell, K. W., Comartin, C. D., Idriss, I. M., Lew, M., Mehrain, M., Moehle, J. P.,
467   Naeim, F., and Sabol, T. A., 2011. Representation of bi-directional ground motions for design
468   spectra in building codes, *Earthquake Spectra* **27**, 927–937.
469 Tezcan, S. S., and Alhan, C., 2001. Parametric analysis of irregular structures under seismic load-
470   ing according to the new Turkish earthquake code, *Engineering Structures* **23**, 600–609.
471 Watson-Lamprey, J., and Boore, D. M., 2007. Beyond SaGMRotI: conversion to SaArb, SaSN,
472   and SaMaxRot, *Bulletin of the Seismological Society of America* **97**, 1511–1524.
473 Wilson, E. L., and Suharwardy, I., 1995. A clarification of the orthogonal effects in a three-
474   dimensional seismic analysis, *Earthquake Spectra* **11**, 659–666.
475 Zamora, M., and Riddell, R., 2011. Elastic and inelastic response spectra considering near-fault
476   effects, *Journal of Earthquake Engineering* **15**, 775–808.